

Surviving Under Pressure: The Role of Solvent, Crystal Size, and Morphology During Pelletization of Metal–Organic Frameworks

Timothy C. Wang,* Ashley M. Wright, William J. Hoover, Kevin J. Stoffel, Rachelle K. Richardson, Stephanie Rodriguez, Roberto C. Flores, John P. Siegfried, Nicolaas A. Vermeulen, Patrick E. Fuller, Mitchell H. Weston, Omar K. Farha, and William Morris*

Cite This: <https://doi.org/10.1021/acsami.1c09619>

Read Online

ACCESS |

Metrics & More

Article Recommendations

Supporting Information

ABSTRACT: As metal–organic frameworks (MOFs) gain traction for applications, such as hydrogen storage, it is essential to form the as-synthesized powder materials into shaped bodies with high packing densities to maximize their volumetric performance. Mechanical compaction, which involves compressing the materials at high pressure, has been reported to yield high monolith density but often results in a significant loss in accessible porosity. Herein, we sought to systematically control (1) crystal size, (2) solvation, and (3) compacting pressure in the pelletization process to achieve high packing density without compromising the porosity that makes MOFs functional. It was determined that solvation is the most critical factor among the three factors examined. Solvation that exceeds the pore volume prevents the framework from collapsing, allowing for porosity to be maintained through pelletization. Higher pelletization pressure results in higher packing density, with extensive loss of porosity being observed at a higher pressure if the solvation is below the pore volume. Lastly, we observed that the morphology and size of the MOF particles result in variation in the highest achievable packing efficiency, but these numbers (75%) are still greater than many existing techniques used to form MOFs. We concluded that the application of pressure through pelletization is a suitable and widely applicable technique for forming high-density MOF-monoliths.

KEYWORDS: metal–organic frameworks, formation, pelletization, formulation, hydrogen storage, monolith



1. INTRODUCTION

Commercial products containing metal–organic frameworks (MOFs) have started to appear on the market after more than two decades of fundamental research on these highly diverse materials.^{1,2} Because of the many advantages that MOFs possess, including high surface area, tunability, and the ease of predicting material properties by in silico simulation, numerous applications have been proposed for MOFs.^{3–7} The applications demonstrated with MOFs include but are not limited to gas storage,^{8–11} separation,^{12,13} catalysis,^{14–16} drug delivery.^{17,18}

Various challenges need to be addressed to develop these early stage research results into commercial products, including large-scale synthesis, material forming, and prototype development. Forming the as-synthesized MOF powders into a suitable-shaped body is an essential step toward any MOF application. Extensive research has been performed by multiple research groups in this area.^{19–24} In these reports, several forming techniques have been examined to generate the optimal form of MOFs for desired applications, including granulation,^{25,26} extrusion,²⁷ spray-drying,²⁸ monolith formation,²⁴ and pelletization.²⁹

Forming methods involving mechanical compaction, such as pelletization, are typically viewed as paths to yield formed materials with high packing efficiency that are particularly desirable for gas storage applications. With several MOFs exhibiting the hydrogen storage capacities that exceed the 2020 goal set by the U.S. Department of Energy,^{30–34} there is an urgent need to form these materials into high-density monoliths without sacrificing their hydrogen storage performance. To realize the MOF-based hydrogen storage at an application scale, pelletization of MOFs has been investigated extensively as the preferred forming technique.

However, because of the generally low mechanical stability, pelletized MOFs usually exhibit a significant loss in porosity as the framework collapses during the high-pressure compaction process.^{22,29,35–44} Since the hydrogen adsorption capacity

Special Issue: Emerging Materials for Catalysis and Energy Applications

Received: May 24, 2021

Accepted: July 28, 2021

60 strongly correlates to the accessible surface area of MOFs,³⁰ a
61 lowered porosity is expected to make a detrimental impact on
62 the hydrogen storage performance. Recently, a few reports
63 suggest that by introducing guest molecules as a removable
64 scaffold in the pores⁴⁵ or solvating the MOFs⁴⁶ used in the
65 mechanical compaction process, formed material with high
66 packing density can be achieved with minimal loss in the
67 structural integrity of the MOF. Inspired by these findings, we
68 sought to better understand MOF pelletization by conducting
69 a systematic study that examines multiple variables during the
70 compaction process.

71 Herein, we present a study that investigates the effect of (1)
72 solvation, (2) pelletization pressure, and (3) crystal size on
73 MOF pelletization. To gain an understanding of the pellet-
74 ization process, we selected two MOFs to study: HKUST-1, a
75 potential candidate for methane storage,¹¹ and Ni₂(*m*-dobdc),
76 a MOF-74 analog that exhibits high heat of adsorption for
77 hydrogen storage.¹³ We show successful forming of monolithic
78 MOF pellets with high packing density while maintaining high
79 porosity. A systematic optimization study reveals MOF
80 solvation is the most critical factor to achieving successful
81 MOF pelletization across two different MOFs. It is also
82 observed that crystal size and morphology have a less
83 pronounced effect on the outcome of pelletization, which
84 will be discussed in detail. Overall, our results show monoliths
85 with excellent packing efficiency (>75%) can be obtained with
86 less than 5% loss in porosity when the pelletization condition is
87 optimized. Since the hydrogen storage performance of MOF
88 strongly correlates to the porosity measured by nitrogen
89 isotherms,⁴⁷ we expect pelletization to be a suitable technique
90 to form MOFs for gas storage applications, particularly for
91 hydrogen storage.

2. EXPERIMENTAL SECTION

92 **2.1. Synthesis of MOF Powder and Control of Crystal Size.**
93 **2.1.1. HKUST-1.** Initially, we prepared HKUST-1 in three different
94 crystal size ranges, large (>425 μm), medium (53–106 μm), and
95 small (1–2 μm) (see Supporting Information, section S2). Briefly, we
96 synthesized the large (>425 μm) and medium (53–106 μm) sized
97 crystals using a solvothermal procedure with acetic acid as the
98 modulator. To obtain the desired HKUST-1 crystal size ranges, we
99 sieved the as-synthesized material using the appropriate sieve screens
100 at the desired mesh size. For small crystal HKUST-1, we generated
101 small (1–2 μm) crystals by adapting a reported synthesis protocol
102 performed at -78 °C.⁴⁸

103 **2.1.2. Ni₂(*m*-dobdc).** For Ni₂(*m*-dobdc), we prepared two
104 different-sized crystal materials, medium-sized (1–2 μm) and small-
105 sized (<100 nm) (see SI, section S2). To prepare micron-sized
106 medium-sized Ni₂(*m*-dobdc), we followed the solvothermal pro-
107 cedure reported by Kapelewski et al.¹³ Whereas, we prepared
108 nanocrystalline small-sized Ni₂(*m*-dobdc) by adapting a room
109 temperature synthesis procedure reported by Garzon-Tovar et al.⁴⁹
110 All synthesized materials were characterized by N₂ adsorption, PXRD
111 and SEM (section S3) before use in the pelletization studies.

112 **2.2. Control of Solvation.** To control the solvation, all
113 synthesized MOFs were fully activated using a vacuum oven and
114 then solvated with methanol to various solvation levels with regard to
115 the pore volume measured by the N₂ adsorption isotherm. Four
116 different solvation levels (0%, 50%, 100%, 150% of pore volume) are
117 examined. The MOF-solvent mixtures were sealed in a vial and
118 equilibrated in a 60 °C oven to ensure an even distribution of solvent.
119 The masses of equilibrated MOF powder samples did not significantly
120 changed after the equilibration process, indicating the correct
121 solvation levels were maintained. Before the pelletization process,
122 the gentle stirring of the solvated powder ensured material
123 homogeneity (see SI section S4).

2.3. Pelletization Procedure. A design of experiments was
124 performed on each MOF to understand the variables that affect
125 pelletization with three factors: (1) pressure, (2) solvation, and (3)
126 crystal size. The pressure was investigated at three levels (9050,
127 45000, 90000 psi), solvation at four levels mentioned above, and
128 crystal size at two (Ni₂(*m*-dobdc) and three (HKUST-1) levels.
129 Finally, each pelletization experiment was performed in triplicate. The
130 volume of the formed pellets was measured geometrically, and the
131 densities were calculated according to the procedure described in
132 section S4. N₂ isotherms were recorded to confirm the structural
133 integrity after compression. 134

3. RESULT AND DISCUSSION

3.1. Effects of Solvation and Pressure in Pelletizing
HKUST-1 (Large Crystals, >425 μm). To understand the
135 effect of applied pressure and MOF solvation during the
136 pelletization process, we investigated how pressure affects
137 pellet density and N₂ uptake (~1 bar at 77 K) at four different
138 solvation levels. The N₂ uptake of the formed MOF pellet is
139 compared to the adsorption performance of the powder, with
140 losses in N₂ uptake indicative of micropore collapse. Figure 1
141 summarizes the structure–function relationship plots (pressure
142 vs N₂ uptake and pellet density) at 0, 50, 100, and 150%
143 solvation for the large crystal (>425 μm) HKUST-1. 144
145

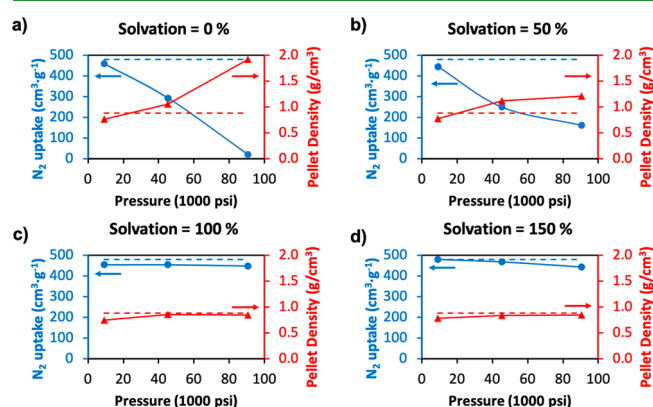


Figure 1. Pelletization results using large crystals (>425 μm) HKUST-1 as the starting material. Pressure–density (red line) and pressure–porosity relationship (blue line) of the formed pellets are plotted in panels a–d, corresponding to solvation level from 0% to 150%. Blue dashed line: Porosity for powder HKUST-1. Red dashed line: Crystallographic density of HKUST-1. All plotted values are the average of three repeated pelletization experiments.

146 Pelletizing with a pressure of 9,050 psi generates pellets with
147 densities of ~0.75 g/cm³ independent of the solvation level.
148 The pellets exhibit densities that are approximately 85% of the
149 crystallographic density (0.88 g·cm⁻³, red dashed line) and
150 maintain >95% of the powder porosity.

151 To further improve pellet densities, we increase the
152 pelletization pressures to 45 000 psi and 90 000 psi. Notably,
153 we observed drastically different effects of pressurization with
154 respect to the solvation levels. At 0% solvation, the pellet
155 densifies with increasing pelletization pressure from 0.75 to
156 1.92 g/cm³ at 9050 and 90 000 psi, respectively (Figure 1a).
157 Pressures greater than 45 000 psi result in monolith densities
158 higher than the crystallographic density of HKUST-1. The
159 increase in monolith density is accompanied by a significant
160 loss in porosity, and the saturated N₂ uptake drops from 480
161 cm³·g⁻¹ (blue dashed line) for powdered MOF to near zero
162 when the pellet is pressed at 90 000 psi, indicating the total

collapse of the MOF micropores. Several other research groups have also reported similar results when pelletizing MOF materials, leading to the conclusion that pelletization might not be suitable for forming MOF materials.

Interestingly, solvating the MOF with methanol improves the pressure–density–porosity correlation. Pelletization of a 50% solvated HKUST-1 (Figure 1b) sample at 45 000 psi results in a volumetric density (1.12 g/cm³) that surpasses the crystallographic density (0.88 g/cm³) with only a 50% loss in porosity. When the pelletization pressure is increased to 90 000 psi, the increase in density levels off (1.21 g/cm³), and the porosity is partially maintained. This result suggests the solvent molecules in the pores prevent the pores from collapsing during the compaction process, which is in line with previous observation.

At above 100% solvation, HKUST-1 pellets with ideal packing efficiency can be made with less than 5% loss in porosity. As shown in Figures 1c and 1d, when applying pressure higher than 45,000 psi in the pelletization procedure, the pellets all exhibited excellent monolith densities (~0.84 g/cm³) corresponding to 95% packing efficiency. After pelletization of HKUST-1 at 150% solvation, we observe wetting of the die set with a trace amount of solvent, indicating that excess solvent in the space between individual crystals is removed from the formed pellets during the compression process. This observation agrees well with the measured solvation of the formed pellets with near-ideal monolith density. When activating these pellets, solvent accounted for 99% and 102% of the pore volume was evacuated, even though the MOF powders were initially solvated at 100% and 150%, respectively. The solvation levels of the pellets correspond the void volume contributed by the micropores of the MOFs and the interstitial space between MOF crystallites. The fact that the solvation levels are very close to 100% of the pore volume of HKUST-1 (99% and 102%) indicates there is very little void space between MOF crystallites, which results in the excellent packing efficiency.

Our results demonstrate that HKUST-1 pellets made at low pressures (<10 000 psi for large crystals HKUST-1) exhibit good pellet densities with low losses in porosity irrespective of the solvation level. However, to maximize the pellet density, compression pressure higher than 45 000 psi is needed for the pelletization process. MOF solvation plays a critical role in maintaining structural integrity, and it was found that solvation levels greater than 100% are necessary for preserving 95% of the nitrogen uptake capacity. This result indicated that the solvent in the MOF pores prevents the MOF structure from collapsing during the high-pressure pelletization process, which also suggests that scaffolding or solvating MOFs protect the pores during the pelletization process. Opposed to previous reports that suggested pelletization is not applicable to HKUST-1 at high pressure, our results showed that pelletization is a suitable technique for forming HKUST-1, as long as the MOF is solvated at a level of 100% or more of the pore volume during the compression process or the pressing pressure is maintained at low-pressure levels (<10 000 psi for large crystals HKUST-1).

3.2. Effects of Crystal Size in Pelletizing HKUST-1. The applicability of pelletization across different crystal sizes is highly desired since it is challenging to control the crystallite size of most MOFs with a reasonable yield. Therefore, a generalizable forming technique for MOFs should be applicable to a range of crystal sizes. To investigate if

pelletization could be applied to different crystal sizes, we performed pelletization studies on large (>425 μm), medium (53–106 μm), and small (1–2 μm) sized HKUST-1 crystals.

To elucidate the effect of crystal size, the pressure–density–porosity relationship for all three crystal sizes is summarized in Figure 2. The large crystal HKUST-1 data presented in Figure

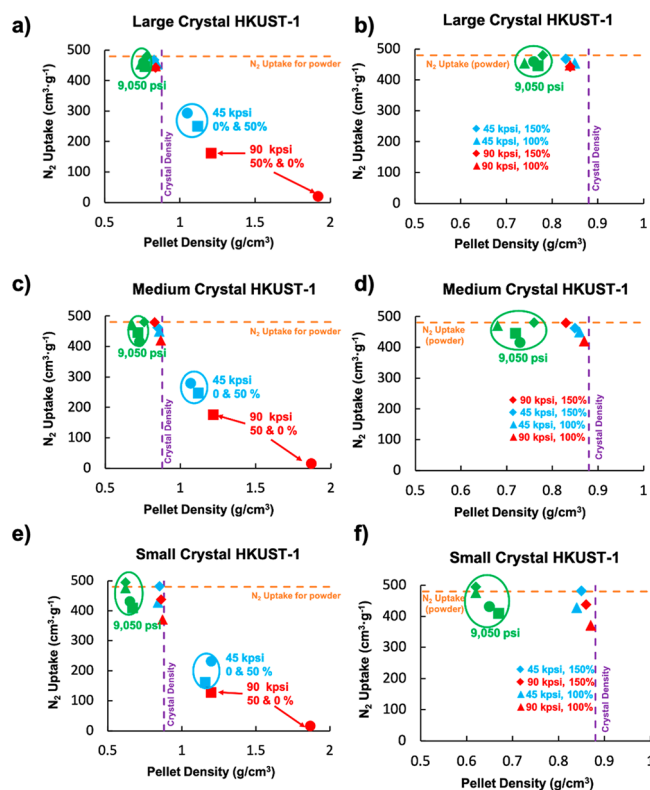


Figure 2. Pelletization results on (a) large (>425 μm) crystal HKUST-1, (c) medium (53–106 μm), and (e) small (1–2 μm) sized HKUST-1. Panels b, d, and f are the respective expanded views of the successful pelletization studies in panels a, c, and e. Pellets pressed at 90 500 psi (green), 45 000 psi (blue), and 90 000 psi (red). 0% solvation (●), 50% solvation (■), 100% solvation (▲), 150% solvation (◆). Purple dashed line: Crystallographic density of HKUST-1. Orange dash line: N₂ uptake for HKUST-1. All plotted values are the average of three repeated pelletization experiments.

1 is condensed into Figure 2a and b. The trend that (1) pelletization at 9050 psi yielded pellets with 85% of the crystallographic density without significant loss of porosity and (2) pellet density representing 95% of crystallographic density is achievable without loss in porosity when the MOF is solvated above 100% solvation and pressed at higher than 45 000 psi can be observed.

A similar trend is observed for the small and medium crystals by comparing Figures 2a, c, and e. However, a few differences in the results are observed with smaller crystal sizes. First, for both small and medium-sized crystals, the pellets pressed at 9,050 psi exhibit observably lower density. The medium-sized HKUST-1 yielded an average pellet density of 0.72 g/cm³, and the small-sized HKUST-1 yielded 0.65 g/cm³, as opposed to 0.75 g/cm³ in the large crystal HKUST-1 trials. In addition, some of these pellets exhibit lowered porosities (~15% loss) when the starting powder is solvated less than 100% solvation. In contrast, the large crystals lost less than 5% of porosity at the same pelletization condition.

251 The lowered pellet densities may reflect the increased
252 difficulty in eliminating the pores between MOF particles. The
253 size of the interstitial spacing decreases as the crystal becomes
254 smaller. Since the smaller interstitial spacings are more
255 mechanically stable, higher pressure is needed in the
256 compression process to eliminate them from the pellets.

257 On the other hand, the decreases in porosity observed for
258 the pellets made from HKUST-1 with smaller crystal size may
259 be attributed to the decreased mechanical stability of the
260 MOF. Because of the faster crystallization rate in the synthesis,
261 the number of defects, such as missing linkers or metal, may be
262 higher in the smaller HKUST-1 crystals. It is well-known in the
263 literature⁴⁰ that defects in the MOF can lower mechanical
264 stability, making the pores more likely to collapse during the
265 compression process.

266 As the pelletization increased to 45 000 and 90 000 psi (blue
267 and red points in Figure 2d and f), an average pellet density of
268 0.85 g/cm³ (97% of crystallographic density) is achieved for
269 the pellets pressed from powders that are solvated above 100%.
270 However, in the tests using medium and small-sized HKUST-
271 1, considerable porosity loss is observed when the condition is
272 not optimized.

273 From the expanded view in Figure 2d and f, the pellets
274 pressed from 100% solvated materials exhibited lower porosity
275 than the 150% solvated material in both medium and small
276 crystals HKUST-1, and the pellets pressed at 90 000 psi lose
277 more N₂ uptake than those pressed at 45 000 psi. Indeed,
278 pelletized at 90 000 psi, the small crystal HKUST-1 loses
279 approximately 20% of porosity, and the medium crystal
280 HKUST-1 lost about 10% of porosity during the compression
281 process. This observation reinforces our assumption that
282 smaller crystal size leads to lower mechanical stability, resulting
283 in more significant pore collapse during the pelletization
284 process.

285 Interestingly, when the solvation is increased to 150% of the
286 pore volume (diamond-shaped points in Figure 2d and f),
287 pellets pressed at high pressures retain their porosities while
288 exhibiting excellent monolith densities, regardless of the crystal
289 size. We propose when the solvation is higher than 150%, the
290 excess solvent in the interstitial spacing acts as a binder to
291 buffer the high compression pressure in the pelletization
292 process. It has been reported in the literature that using
293 binders in the pelletization process reduces the structure
294 degradation during the pelletization process.^{40,43} In contrast to
295 typical binders, the excess solvent can be removed from the
296 pellets during the activation process, resulting in pellets that
297 are essential binder-free. The binder-free feature prevents the
298 loss in overall porosity due to the addition of a nonporous
299 binder. Therefore, nearly complete retention of porosity was
300 achieved in our studies on pelletization of HKUST-1. To sum
301 up, our results support the best conditions for HKUST-1
302 pelletization is at pressures higher than 45 000 psi and with
303 MOF solvation greater than 100% of the pore volume.

304 The fact that monolithic HKUST-1 pellets can be made at
305 near crystallographic density without significant loss in
306 porosity suggests that pelletization is an ideal way of producing
307 high-density formed HKUST-1 for gas storage applications.
308 Further, the applicability of the pelletization technique over a
309 wide range of crystal sizes (from 0.5 mm to 1 μm) alleviates
310 the need for optimizing the synthesis procedure, which makes
311 the overall production of formed HKUST-1 pellets readily
312 feasible.

313 **3.3. Results on Pelletization of Ni₂(*m*-dobdc).** Spurred
314 by our results from the pelletization of HKUST-1, we further
315 investigated the applicability of pelletization for forming other
316 MOFs. Using the same methodology for HKUST-1, we
317 identified the conditions to pelletize Ni₂(*m*-dobdc) into high-
318 density monoliths without significantly reducing microporos-
319 ity. Two different crystal sizes of Ni₂(*m*-dobdc) were prepared
320 for the study. The synthesized powder materials are solvated
321 with methanol at 0%, 50%, 100%, and 150% of the pore
322 volume to examine the effect of solvation level. The pressure–
323 density–porosity relationship was plotted in Figure 3 for
324 pellets produced from medium-sized (1–2 μm) and small-
325 sized (<100 nm) crystals.

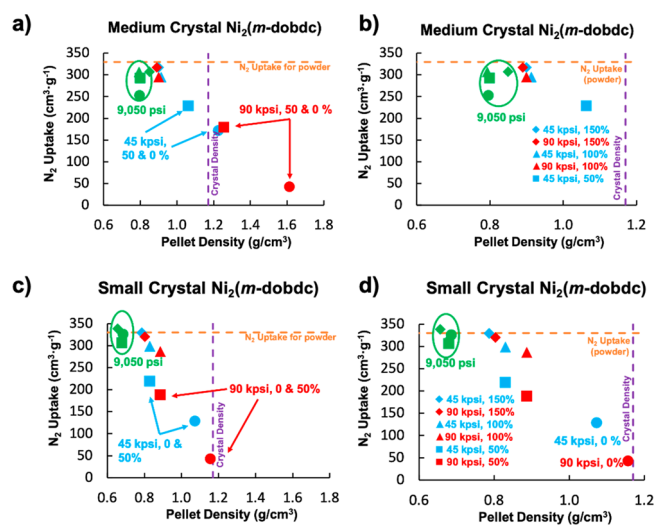


Figure 3. Pelletization results using (a) medium crystals (1–2 μm) Ni₂(*m*-dobdc) and (c) small crystals (<100 nm) Ni₂(*m*-dobdc) as the starting material. Panels b and d are expanded views of panels a and c. Pellets pressed at 9050 psi (green), 45 000 psi (blue), and 90 000 psi (red). 0% solvation (●), 50% solvation (■), 100% solvation (▲), 150% solvation (◆). Purple dashed line: Crystallographic density of Ni₂(*m*-dobdc). Orange dashed line: N₂ uptake for Ni₂(*m*-dobdc). All plotted values are the average of three repeated pelletization experiments.

The pelletization results for medium-sized Ni₂(*m*-dobdc) 326 (Figure 3a and b) reveal a similar trend compared to HKUST-
327 1 results. Pelletization at 9 050 psi yielded lower pellet density
328 (0.81 g/cm³), and the under-solvated powder leads to some
329 loss in porosity after compression. Increasing the pressure to
330 45 000 psi and above leads to more drastic losses in porosity
331 when the solvation level is lower than 100%. The extent of
332 porosity loss becomes more significant when the solvation is
333 lower and when the pressure is higher. Mirroring the learning
334 from the HKUST-1 results, the best solvation for pelletization
335 is 150% of the pore volume for medium crystal Ni₂(*m*-dobdc).
336 (Figure 3b). Pellet density of 0.90 g/cm³ was achieved without
337 loss in the overall porosity for the formed pellets. However,
338 unlike the 97% crystallographic density achieved in the
339 HKUST-1 study, the highest pellet density achieved by
340 pelletizing medium-sized crystals (1–2 μm) of Ni₂(*m*-dobdc)
341 reaches 77% of the crystallographic density. 342

343 Interestingly, the results for pelletizing the small crystal
344 (<100 nm) Ni₂(*m*-dobdc) showed some distinct differences
345 (Figure 3c and d). At 9050 psi, the pellet densities (0.68 g/
346 cm³) are lower than the medium-sized crystal Ni₂(*m*-dobdc). 346

347 This result is in line with the size effect observed in the
348 HKUST-1 studies that the smaller crystals are more difficult to
349 pack and leads to lower pellet densities. As the pressure
350 increase to 45 000 psi and above, significant porosity loss is
351 observed for the pellets pressed from 0 and 50% solvated
352 Ni₂(*m*-dobdc). However, the pellet density did not increase as
353 much when compared to the corresponding medium crystal
354 results.

355 Again, the best condition for pelletizing small crystal (<100
356 nm) Ni₂(*m*-dobdc) is pressing 150% solvated MOF powders at
357 45 000 psi or higher, but the highest density pellets produced
358 without porosity loss reach only 68% of the crystallographic
359 density at the best condition (Figure 3d, diamond-shaped
360 points in blue and red).

361 The results for pelletizing Ni₂(*m*-dobdc) suggest the highest
362 achievable pellet density is MOF-dependent, and the wide
363 applicability of pelletization across different crystal sizes
364 observed in the HKUST-1 studies may not be applicable for
365 extremely small MOF crystals at the nanometer scale.

366 **3.4. Discussion of Morphology and Size Effect on**
367 **Pelletization.** Although the outcome for pelletization of
368 Ni₂(*m*-dobdc) was not as good as that of HKUST-1, the result
369 suggested a general trend for pelletization of MOF powder that
370 is transferable between different MOFs. From the two MOF
371 examples investigated, to reach high pellet density without
372 losing the porosity, MOFs must be solvated at greater than
373 100% of the pore volume, and the pellets should be pressed at
374 a pressure higher than 45 000 psi. To explain the difference in
375 the HKUST-1 and Ni₂(*m*-dobdc) results, we hypothesize the
376 morphology and size of the MOF crystals may affect the
377 outcome of pelletization.

378 Synthesized as needle-shaped crystals, Ni₂(*m*-dobdc) is
379 crystallized in a hexagonal space group, while HKUST-1 in a
380 highly symmetrical cubic space group. Therefore, it is
381 anticipated that there will be an anisotropic orientation of
382 crystallite domains in the pellets of Ni₂(*m*-dobdc). In this case,
383 the interstitial space is more difficult to remove by simply
384 applying mechanical pressure. Highly symmetric cubic
385 HKUST-1 does not encounter this issue; thus, higher packing
386 efficiency is achieved.

387 The overall lower densities achieved by the small crystal
388 Ni₂(*m*-dobdc) can be explained by the extremely small
389 crystallite size in the nanometer range. When particles of
390 similar size pack together, the size of the interstitial voids
391 between the matters are in the same order of magnitude as the
392 particles. Therefore, it is expected that to pack nanocrystalline
393 MOFs, a lot of pores that are less than 100 nm will need to be
394 eliminated during the pelletization process. We hypothesize
395 the smaller size of the interstitial pores is more likely to be
396 supported by excess solvent during the compression process.
397 The retention of these pores can lead to lower packing
398 efficiency for the forming process. Therefore, pelletization may
399 be less effective in maximizing the packing efficiency when
400 used to form nanocrystalline MOFs.

401 Overall, the results for Ni₂(*m*-dobdc) suggested pelletization
402 is an effective technique for forming Ni₂(*m*-dobdc) into high-
403 density monoliths, albeit the result was not as outstanding as
404 the pelletization studies on HKUST-1. Packing density
405 representing >75% of the crystallographic density was achieved
406 with the medium-sized crystals, which is excellent compared to
407 many other forming techniques. What's more, the porosity for
408 the formed monolith is fully maintained, which is often not

achievable with other forming techniques that require binder
addition. 409 410

4. CONCLUSION

MOFs have shown great potential at solving the grand
challenge of hydrogen storage by reaching the material target
set by the U.S. Department of Energy. To realize this
performance at an application level, it is essential to pack the
MOFs into high-density monoliths. From this study, we
concluded that pelletization is a suitable and generally
applicable technique for forming high-density MOF monoliths.
We have identified that MOF solvation during pelletization as
the most critical factor in preventing porosity loss and
framework collapse during the compaction process. In
addition, we have explored how pressure and crystallite size
affect the pelletization process. The compression pressure did
not affect the outcome as long as the pores are fully solvated
with solvent. Although we demonstrated that crystallite size
and morphology could lead to a difference in packing
efficiencies, these numbers are still excellent (>75%) compared
to many existing techniques to form MOFs. These results are
in contrast to previous results that have highlighted the
underlying MOF as the failure mechanism for transformation
performed under pressure. 411 412 413 414 415 416 417 418 419 420 421 422 423 424 425 426 427 428 429 430

■ ASSOCIATED CONTENT

SI Supporting Information

The Supporting Information is available free of charge at
<https://pubs.acs.org/doi/10.1021/acsami.1c09619>.

Material and instrumentation, detailed synthesis procedure,
characterizations of MOF powders, detailed resolution and
pelletization procedure, and pressure–density–porosity
relationship of HKUST-1 (medium and small crystals) and
Ni₂(*m*-dobdc) (medium and small crystals) (PDF) 431 432 433 434 435 436 437 438 439 440

■ AUTHOR INFORMATION

Corresponding Authors

William Morris – NuMat Technologies, Skokie, Illinois 60077,
United States; orcid.org/0000-0003-2818-4406;
Email: william@numat-tech.com

Timothy C. Wang – NuMat Technologies, Skokie, Illinois
60077, United States; orcid.org/0000-0002-2736-2488;
Email: t.wang@numat-tech.com

Authors

Ashley M. Wright – NuMat Technologies, Skokie, Illinois
60077, United States; orcid.org/0000-0002-9475-2638

William J. Hoover – NuMat Technologies, Skokie, Illinois
60077, United States

Kevin J. Stoffel – NuMat Technologies, Skokie, Illinois 60077,
United States

Rachelle K. Richardson – NuMat Technologies, Skokie,
Illinois 60077, United States

Stephanie Rodriguez – NuMat Technologies, Skokie, Illinois
60077, United States

Roberto C. Flores – NuMat Technologies, Skokie, Illinois
60077, United States

John P. Siegfried – NuMat Technologies, Skokie, Illinois
60077, United States

Nicolaas A. Vermeulen – NuMat Technologies, Skokie,
Illinois 60077, United States

466 Patrick E. Fuller – NuMat Technologies, Skokie, Illinois
467 60077, United States
468 Mitchell H. Weston – NuMat Technologies, Skokie, Illinois
469 60077, United States; orcid.org/0000-0002-4574-5888
470 Omar K. Farha – NuMat Technologies, Skokie, Illinois 60077,
471 United States; Department of Chemistry and International
472 Institute for Nanotechnology and Department of Chemical
473 and Biological Engineering, Northwestern University,
474 Evanston, Illinois 60208, United States; orcid.org/0000-0002-9904-9845
475

476 Complete contact information is available at:
477 <https://pubs.acs.org/10.1021/acsami.1c09619>

478 Notes

479 The authors declare the following competing financial
480 interest(s): The authors have a financial interest in NuMat
481 Technologies, a startup company that is commercializing
482 metal-organic frameworks.

483 ACKNOWLEDGMENTS

484 The authors gratefully acknowledge the support from the U.S.
485 Department of Energy (DOE) SBIR/STTR Program and the
486 Hydrogen and Fuel Cell Technology Office (DE-SC0018532).

487 REFERENCES

488 (1) Mueller, U.; Schubert, M.; Teich, F.; Puetter, H.; Schierle-Arndt,
489 K.; Pastré, J. Metal–Organic Frameworks-Prospective Industrial
490 Applications. *J. Mater. Chem.* **2006**, *16*, 626–636.
491 (2) Farha, O. K.; Chen, Z.; Wasson, M. C.; Drout, R. J.; Robison, L.;
492 Idrees, K.; Knapp, J. G.; Son, F. A.; Zhang, X.; Hierse, W.; Kühn, C.;
493 Marx, S.; Hernandez, B. The State of the Field: From Inception to
494 Commercialization of Metal–Organic Frameworks. *Faraday Discuss.*
495 **2021**, *225*, 9–69.
496 (3) Férey, G. Hybrid Porous Solids: Past, Present, Future. *Chem. Soc.*
497 *Rev.* **2008**, *37*, 191–214.
498 (4) Furukawa, H.; Müller, U.; Yaghi, O. M. Heterogeneity within
499 Order” in Metal–Organic Frameworks. *Angew. Chem., Int. Ed.* **2015**,
500 *54*, 3417–3430.
501 (5) Kitagawa, S.; Kitaura, R.; Noro, S. Functional Porous
502 Coordination Polymers. *Angew. Chem., Int. Ed.* **2004**, *43*, 2334–2375.
503 (6) Zhou, H. C.; Long, J. R.; Yaghi, O. M. Introduction to Metal–
504 Organic Frameworks. *Chem. Rev.* **2012**, *112*, 673–674.
505 (7) Furukawa, H.; Cordova, K. E.; O’Keeffe, M.; Yaghi, O. M. The
506 Chemistry and Applications of Metal–Organic Frameworks. *Science*
507 **2013**, *341*, 1230444.
508 (8) Li, H.; Wang, K.; Sun, Y.; Lollar, C. T.; Li, J.; Zhou, H. C.
509 Recent Advances in Gas Storage and Separation Using Metal–
510 Organic Frameworks. *Mater. Today* **2018**, *21*, 108–121.
511 (9) Suh, M. P.; Park, H. J.; Prasad, T. K.; Lim, D. W. Hydrogen
512 Storage in Metal–Organic Frameworks. *Chem. Rev.* **2012**, *112*, 782–
513 835.
514 (10) García-Holley, P.; Schweitzer, B.; Islamoglu, T.; Liu, Y.; Lin, L.;
515 Rodriguez, S.; Weston, M. H.; Hupp, J. T.; Gómez-Gualdrón, D. A.;
516 Yildirim, T.; Farha, O. K. Benchmark Study of Hydrogen Storage in
517 Metal–Organic Frameworks under Temperature and Pressure Swing
518 Conditions. *ACS Energy Lett.* **2018**, *3*, 748–754.
519 (11) Peng, Y.; Krungleviciute, V.; Eryazici, I.; Hupp, J. T.; Farha, O.
520 K.; Yildirim, T. Methane Storage in Metal–Organic Frameworks:
521 Current Records, Surprise Findings, and Challenges. *J. Am. Chem. Soc.*
522 **2013**, *135*, 11887–11894.
523 (12) Li, J. R.; Sculley, J.; Zhou, H. C. Metal–Organic Frameworks
524 for Separations. *Chem. Rev.* **2012**, *112*, 869–932.
525 (13) Kapelewski, M. T.; Geier, S. J.; Hudson, M. R.; Stück, D.;
526 Mason, J. A.; Nelson, J. N.; Xiao, D. J.; Hulvey, Z.; Gilmour, E.;
527 FitzGerald, S. A.; Head-Gordon, M.; Brown, C. M.; Long, J. R. $M_2(m-528$
Dobdc) (M = Mg, Mn, Fe, Co, Ni) Metal–Organic Frameworks

Exhibiting Increased Charge Density and Enhanced H₂ Binding at the
Open Metal Sites. *J. Am. Chem. Soc.* **2014**, *136*, 12119–12129. 529
(14) Yoon, M.; Srirambalaji, R.; Kim, K. Homochiral Metal–
Organic Frameworks for Asymmetric Heterogeneous Catalysis. *Chem.* 530
Rev. **2012**, *112*, 1196–1231. 533
(15) Doonan, C. J.; Sumbly, C. J. Metal–Organic Framework
Catalysis. *CrystEngComm* **2017**, *19*, 4044–4048. 534
(16) Lee, J.; Farha, O. K.; Roberts, J.; Scheidt, K. A.; Nguyen, S. T.;
Hupp, J. T. Metal–Organic Framework Materials as Catalysts. *Chem.* 535
Soc. Rev. **2009**, *38*, 1450–1459. 538
(17) Wu, M. X.; Yang, Y. W. Metal–Organic Framework (MOF)-
Based Drug/Cargo Delivery and Cancer Therapy. *Adv. Mater.* **2017**, 539
29, 1606134. 541
(18) Wang, L.; Zheng, M.; Xie, Z. Nanoscale Metal–Organic
Frameworks for Drug Delivery: A Conventional Platform with New
Promise. *J. Mater. Chem. B* **2018**, *6*, 707–717. 542
(19) Lee, U.-H.; Valekar, A. H.; Hwang, Y. K.; Chang, J.-S. 543
Granulation and Shaping of Metal–Organic Frameworks. In *The* 544
Chemistry of Metal–Organic Frameworks: Synthesis, Characterization, 545
and Applications; Wiley-VCH Verlag GmbH & Co. KGaA: Weinheim, 546
Germany, 2016; pp 551–572. DOI: 10.1002/9783527693078.ch18. 549
(20) Hesse, M.; Mueller, U.; Yaghi, O. Shaped Bodies Containing
Metal–Organic Frameworks. US 7524444B2, April 28, 2009. 550
(21) Chang, J.-S.; Lee, U.-H.; Hwang, Y. K.; Hwang, D. W.; Seo, Y.-
K.; Lee, J. S.; Yoon, J. W.; Shim, K. E. Complex Comprising
Crystalline Hybrid Nanoporous Material Powder. US 9302258B2, 551
April 5, 2016. 555
(22) Bazer-Bachi, D.; Assié, L.; Lecocq, V.; Harbuzaru, B.; Falk, V. 556
Towards Industrial Use of Metal–Organic Framework: Impact of
Shaping on the MOF Properties. *Powder Technol.* **2014**, *255*, 52–59. 558
(23) Ren, J.; Langmi, H. W.; North, B. C.; Mathe, M. Review on
Processing of Metal–Organic Framework (MOF) Materials towards
System Integration for Hydrogen Storage. *Int. J. Energy Res.* **2015**, *39*, 559
607–620. 562
(24) Connolly, B. M.; Madden, D. G.; Wheatley, A. E. H.; Fairen-
Jimenez, D. Shaping the Future of Fuel: Monolithic Metal–Organic
Frameworks for High-Density Gas Storage. *J. Am. Chem. Soc.* **2020**, 563
142, 8541–8549. 566
(25) Valekar, A. H.; Cho, K.-H.; Lee, U.-H.; Lee, J. S.; Yoon, J. W.;
Hwang, Y. K.; Lee, S. G.; Cho, S. J.; Chang, J.-S. Shaping of Porous
Metal–Organic Framework Granules Using Mesoporous γ -Alumina as
a Binder. *RSC Adv.* **2017**, *7*, 55767–55777. 569
(26) Kim, P. J.; You, Y. W.; Park, H.; Chang, J. S.; Bae, Y. S.; Lee, C. 570
H.; Suh, J. K. Separation of SF₆ from SF₆/N₂ Mixture Using Metal–
Organic Framework MIL-100(Fe) Granule. *Chem. Eng. J.* **2015**, *262*, 571
683–690. 574
(27) Ferreira, A. F. P.; Santos, J. C.; Plaza, M. G.; Lamia, N.;
Loureiro, J. M.; Rodrigues, A. E. Suitability of Cu-BTC Extrudates for
Propane-Propylene Separation by Adsorption Processes. *Chem. Eng. J.* 575
2011, *167*, 1–12. 578
(28) Carné-Sánchez, A.; Imaz, I.; Cano-Sarabia, M.; Maspoch, D. A
Spray-Drying Strategy for Synthesis of Nanoscale Metal–Organic
Frameworks and Their Assembly into Hollow Superstructures. *Nat.* 580
Chem. **2013**, *5*, 203–211. 582
(29) Zacharia, R.; Cossement, D.; Lafi, L.; Chahine, R. Volumetric
Hydrogen Sorption Capacity of Monoliths Prepared by Mechanical
Densification of MOF-177. *J. Mater. Chem.* **2010**, *20*, 2145–2151. 583
(30) Allendorf, M. D.; Hulvey, Z.; Gennett, T.; Ahmed, A.; Autrey, 584
T.; Camp, J.; Seon Cho, E.; Furukawa, H.; Haranczyk, M.; Head-
Gordon, M.; Jeong, S.; Karkamkar, A.; Liu, D. J.; Long, J. R.; Meihaus, 585
K. R.; Nayyar, I. H.; Nazarov, R.; Siegel, D. J.; Stavila, V.; Urban, J. J.;
Veccham, S. P.; Wood, B. C. An Assessment of Strategies for the
Development of Solid-State Adsorbents for Vehicular Hydrogen
Storage. *Energy Environ. Sci.* **2018**, *11*, 2784–2812. 589
(31) Farha, O. K.; Özgür Yazaydin, A.; Eryazici, I.; Malliakas, C. D.;
Hauser, B. G.; Kanatzidis, M. G.; Nguyen, S. T.; Snurr, R. Q.; Hupp, J. 590
T. De Novo Synthesis of a Metal–Organic Framework Material
Featuring Ultrahigh Surface Area and Gas Storage Capacities. *Nat.* 591
Chem. **2010**, *2*, 944–948. 597

- 598 (32) Koh, K.; Van Oosterhout, J. D.; Roy, S.; Wong-Foy, A. G.;
599 Matzger, A. J. Exceptional Surface Area from Coordination
600 Copolymers Derived from Two Linear Linkers of Differing Lengths.
601 *Chem. Sci.* **2012**, *3*, 2429–2432.
- 602 (33) Ahmed, A.; Seth, S.; Purewal, J.; Wong-Foy, A. G.; Veenstra,
603 M.; Matzger, A. J.; Siegel, D. J. Exceptional Hydrogen Storage
604 Achieved by Screening Nearly Half a Million Metal–Organic
605 Frameworks. *Nat. Commun.* **2019**, *10*, 1–9.
- 606 (34) Prasad, T. K.; Suh, M. P. Control of Interpenetration and Gas-
607 Sorption Properties of Metal–Organic Frameworks by a Simple
608 Change in Ligand Design. *Chem. - Eur. J.* **2012**, *18*, 8673–8680.
- 609 (35) Domán, A.; Madarász, J.; Sáfrán, G.; Wang, Y.; László, K.
610 Copper Benzene-1,3,5-Tricarboxylate (HKUST-1)-Graphene Oxide
611 Pellets for Methane Adsorption. *Microporous Mesoporous Mater.* **2021**,
612 *316*, 110948.
- 613 (36) Hindocha, S.; Poulston, S. Study of the Scale-up, Formulation,
614 Ageing and Ammonia Adsorption Capacity of MIL-100(Fe), Cu-BTC
615 and CPO-27(Ni) for Use in Respiratory Protection Filters. *Faraday*
616 *Discuss.* **2017**, *201*, 113–125.
- 617 (37) Peterson, G. W.; Decoste, J. B.; Glover, T. G.; Huang, Y.;
618 Jasuja, H.; Walton, K. S. Effects of Pelletization Pressure on the
619 Physical and Chemical Properties of the Metal–Organic Frameworks
620 $\text{Cu}_3(\text{BTC})_2$ and UiO-66. *Microporous Mesoporous Mater.* **2013**, *179*,
621 48–53.
- 622 (38) Chanut, N.; Wiersum, A. D.; Lee, U.-H.; Hwang, Y. K.; Ragon,
623 F.; Chevreau, H.; Bourrelly, S.; Kuchta, B.; Chang, J.-S.; Serre, C.;
624 Llewellyn, P. L. Observing the Effects of Shaping on Gas Adsorption
625 in Metal–Organic Frameworks. *Eur. J. Inorg. Chem.* **2016**, *2016*,
626 4416–4423.
- 627 (39) Alcañiz-Monge, J.; Trautwein, G.; Pérez-Cadenas, M.; Román-
628 Martínez, M. C. Effects of Compression on the Textural Properties of
629 Porous Solids. *Microporous Mesoporous Mater.* **2009**, *126*, 291–301.
- 630 (40) Dhainaut, J.; Avci-Camur, C.; Troyano, J.; Legrand, A.;
631 Canivet, J.; Imaz, I.; Maspoch, D.; Reinsch, H.; Farrusseng, D.
632 Systematic Study of the Impact of MOF Densification into Tablets on
633 Textural and Mechanical Properties. *CrystEngComm* **2017**, *19*, 4211–
634 4218.
- 635 (41) Purewal, J. J.; Liu, D.; Yang, J.; Sudik, A.; Siegel, D. J.; Maurer,
636 S.; Müller, U. Increased Volumetric Hydrogen Uptake of MOF-5 by
637 Powder Densification. *Int. J. Hydrogen Energy* **2012**, *37*, 2723–2727.
- 638 (42) Ursueguía, D.; Díaz, E.; Ordóñez, S. Densification-Induced
639 Structure Changes in Basolite MOFs: Effect on Low-Pressure CH_4
640 Adsorption. *Nanomaterials* **2020**, *10*, 1089.
- 641 (43) Kim, J.; Kim, S.-H.; Yang, S.-T.; Ahn, W.-S. Bench-Scale
642 Preparation of $\text{Cu}_3(\text{BTC})_2$ by Ethanol Reflux: Synthesis Optimization
643 and Adsorption/Catalytic Applications. *Microporous Mesoporous*
644 *Mater.* **2012**, *161*, 48–55.
- 645 (44) Nandasiri, M. I.; Jambovane, S. R.; McGrail, B. P.; Schaefer, H.
646 T.; Nune, S. K. Adsorption, Separation, and Catalytic Properties of
647 Densified Metal–Organic Frameworks. *Coord. Chem. Rev.* **2016**, *311*,
648 38–52.
- 649 (45) Fuller, P.; Weston, M. H.; Morris, W.; Hoover, W. Formation
650 of High Surface Area Metal–Organic Frameworks. US 9925516B2,
651 March 27, 2018.
- 652 (46) Xu, C.; Purewal, J.; Veenstra, M. J. Solvent-Supported
653 Compaction of Metal–Organic Frameworks. US 9757710B1,
654 September 12, 2017.
- 655 (47) Suh, M. P.; Park, H. J.; Prasad, T. K.; Lim, D.-W. Hydrogen
656 Storage in Metal–Organic Frameworks. *Chem. Rev.* **2012**, *112*, 782–
657 835.
- 658 (48) Wee, L. H.; Lohe, M. R.; Janssens, N.; Kaskel, S.; Martens, J. A.
659 Fine Tuning of the Metal–Organic Framework $\text{Cu}_3(\text{BTC})_2$ HKUST-
660 1 Crystal Size in the 100 nm to 5 Micron Range. *J. Mater. Chem.*
661 **2012**, *22*, 13742–13746.
- 662 (49) Garzón-Tovar, L.; Carné-Sánchez, A.; Carbonell, C.; Imaz, I.;
663 Maspoch, D. Optimised Room Temperature, Water-Based Synthesis
664 of CPO-27-M Metal–Organic Frameworks with High Space-Time
665 Yields. *J. Mater. Chem. A* **2015**, *3*, 20819–20826.